COMMUNICATION

Tandem catalysis by ultrathin metal-organic nanosheets formed through post-synthetic functionalisation of a layered framework

Joshua Nicks,[a] Jiawen Zhang [a] and Jonathan A. Foster*[a]

Received 00th January 20xx,
Accepted 00th January 20xx

DOI: 10.1039/x0xx00000x

Covalent post-synthetic functionalisation of layered metal-organic frameworks is demonstrated as a new approach to forming ultrathin nanosheets for use in catalysis. An aminoterephthalate framework was partially functionalised with sulfonate chains and exfoliated to form predominantly monolayer nanosheets able to catalyse a two-step acid-base reaction in one pot.

Metal-organic nanosheets (MONs) are an exciting new class of two-dimensional (2D) nanomaterial with tunable, periodic structures that lend themselves to numerous applications, including: molecular separation, sensing and electronics.[1–5] In particular, their high external surface areas, exposed active sites and ease of recovery make them ideal candidates for use as catalysts and MONs have been shown to outperform their bulk counterparts, metal-organic frameworks (MOFs), in a range of reactions.[6–14]

MONs can be fabricated directly from their molecular building blocks or by exfoliation of a layered MOF, described as bottom-up and top-down approaches respectively. In the latter, energy is added to overcome weak interlayer interactions and exfoliate the nanosheets whilst minimising disruption to the in-plane bonding which leads to fragmentation. Liquid-assisted ultrasonication has become the most commonly used top-down method due to its ease of setup and scalability,[15–19] though other techniques have also been used to produce few-layer sheets.[20–23] A number of groups have also demonstrated enhanced exfoliation by intercalating groups between layers to further weaken these inter-layer interactions.[13,24,25]

Post-synthetic functionalisation (PSF), in which new functionalities are introduced following assembly of the metal-organic material, provides an attractive pathway to tuning the structure and properties of MONs.[26,27] Examples of MON PSF through coordination of ligand, solvent molecules or metal-ions have been demonstrated.[28,29] However, to our knowledge, no studies have been undertaken into the effect of covalent PSF on MONs. Covalent functionalisation offers the advantages of a stable covalent bond rather than a more labile dative bond, meaning functionalisation is typically more robust.[30,31] A range of covalent PSF chemistries have already been developed and used to introduce functionalities to other metal-organic materials.[27] In particular, covalent PSF of amino functionalised MOFs has been thoroughly studied, due to the variety of reactions in which amines serve as nucleophiles.[31]

We hypothesised that covalent PSF of a layered MOF could be used to enhance exfoliation and introduce new catalytically active functionalities onto the surface of the resulting MON. In particular, we predicted that functionalisation of copper 2-aminobenzenedicarboxylate, Cu(ABDC)(DMF), with 1,3-propanesultone would introduce repulsive charges between the layers, aiding exfoliation and creating acidic and basic active sites for catalysis (figure 1).

Copper acetate monohydrate and 2-aminobenzene-1,4-dicarboxylic acid (ABDC) were heated in DMF at 100 °C for 18 h in a sealed reaction vial. Elemental and thermogravimetric analysis of the resulting green microcrystalline powder (96% yield) confirmed the materials composition to be consistent with the expected formula, Cu(ABDC)(DMF) (figs. S1-4). Pawley refinement of the powder X-ray diffraction pattern (fig. S5) obtained from the material showed the structure is isostructural with the known crystal structure of MOF-46 (Zn(ABDC)(DMF)). Cu (ABDC)(DMF) therefore has a layered structure in which four ABDC linkers coordinate to the M_2-paddlewheel (PW) and interconnect these units in the 2D **sql** topology, while DMF coordinates to the PW axial sites. Hence, the lamellar structure features strong metal-carboxylate bonding within the layers, with disordered amine groups providing weak interlayer hydrogen bonding.

Cu(ABDC)(DMF) was post-synthetically functionalised by treating a suspension of the MOF in chloroform with a 10 molar excess of 1,3-propanesultone and stirring at 55 °C. Cu(ABDC-PS)(DMF) was obtained as a lighter green powder after 1 week (fig. 1a). Comparison of experimental PXRD patterns confirmed the layered structure had been maintained and no change in the interlayer distance was observed (fig. S9). Multiple analytical methods evidenced that PSF had taken place. FT-IR measurements of Cu(ABDC)(DMF) and Cu(ABDC-PS)(DMF) gave

[a] *University of Sheffield, Department of Chemistry, Sheffield, UK. Email: jona.foster@sheffield.ac.uk*

† Electronic Supplementary Information (ESI) available: full experimental details, synthetic procedures, exfoliation studies and catalytic data. See DOI: 10.1039/x0xx00000x

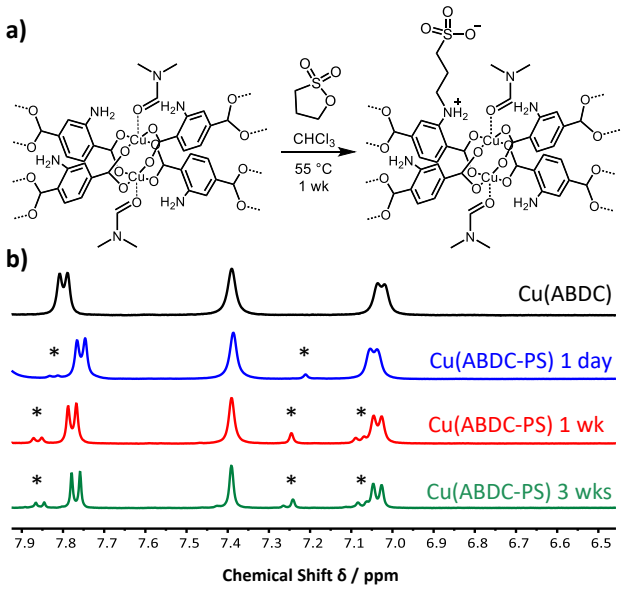

Figure 1. a) Reaction scheme showing the conditions in which Cu(ABDC)(DMF) was functionalised with 1,3-propanesultone to obtain Cu(ABDC-PS)(DMF). b) Comparison between the aromatic regions of ^{1}H NMR spectra of digested samples of [from top to bottom] Cu(ABDC)(DMF) (black) and Cu(ABDC-PS)(DMF) after functionalisation for 1 day (blue), 1 week (red) and 3 weeks (green). Asterisks indicate peaks associated with the functionalised linker. Full spectra can be seen in the ESI, section S2.

similar spectra, though the latter possessed peaks at 1212 cm^{-1} and 1040 cm^{-1} associated with the sulfonate group introduced (fig. S7).[32–34] Weak bands were also observed in the region of 3300-3000 cm^{-1}, associated with introduced C-H stretches. Mass spectrometry of the MOF after acid digestion indicated the presence of both the functionalised ([M]$^-$ = 302.0, [M+Na]$^-$ = 324.0) and unfunctionalised linker ([M]$^-$ = 180.0).

The degree of conversion was determined using ^{1}H NMR spectroscopy, in which the functionalised and unfunctionalised MOFs were digested with DCl/d_6-DMSO solution (fig. 1b). Integration of the aromatic protons indicated 17% conversion of the secondary amines. PSF was also performed under the same conditions for 1 day and for 3 weeks, giving 6% and 20% conversion respectively. The MOFs were also first desolvated by soaking in acetonitrile for 3 days followed by PSF for 1 day or 1 week, which resulted in 21% and 25% functionalisation respectively (fig. S10). The relatively low degrees of conversion are attributed to the lack of void space within this relatively dense MOF (fig. S11). The samples following PSF of Cu(ABDC)(DMF) for 1 week were used for all remaining studies.

Mass spectrometry also indicates the formation of a difunctionalised species ([M]$^-$ = 424.0, 11 % wrt 302.0), which is thought to be due to the reaction of 1,3-propanesultone with the terminal carboxylic acids of the MOF. Peaks associated with this product were not observed directly in ^{1}H NMR spectra, however aliphatic protons consistent with 3-hydroxypropane-1-sulfonic acid were observed and thought to be formed due to partial hydrolysis of the ester in the acidic NMR solvent system. These sites integrate to approximately 6% of total amine sites.

In order to compare the effect of PSF on exfoliation, the functionalised and unfunctionalised MOFs were each suspended in acetonitrile and subject to 80 kHz ultrasound for 12 hours at ~18°C (see ESI S3.1). Samples were then centrifuged for 1 hour at 1500 rpm to remove larger fragments and leave only nanosheets in suspension. Our initial intention was to exfoliate the material into water. Unfortunately, unlike other Cu-PW MONs we've developed, Cu(ABDC) dissolved in water. Acetonitrile was therefore chosen as the exfoliation medium, as previous studies have demonstrated it to be a good candidate for copper benzenedicarboxylate-based systems.[18,19]

Both Cu(ABDC)(DMF) and Cu(ABDC-PS)(DMF) exfoliated well into acetonitrile. Each suspension exhibited strong Tyndall scattering indicating the presence of nanoparticles (fig. S12). The functionalised suspensions appeared more transparent and this was reflected by weaker absorption in the UV-vis spectra with extinction coefficients of 4285 and 1451 dm^{3}mol^{-1}cm^{-1} for Cu(ABDC)(DMF) and Cu(ABDC-PS)(DMF) respectively. UV-Vis spectroscopy was also used to estimate the concentration of the two suspensions which were both calculated to be 0.4 mgmL^{-1} (figs. S16-18), corresponding to ~50% of the dispersed material remaining in suspension following centrifugation.

The suspensions were drop-cast onto hot mica sheets for AFM imaging (fig. 2). Cu(ABDC)(DMF) nanosheets had rectangular morphologies and a broad particle size distribution, with an average thickness of 25 nm (SD ±19) and average lateral size of 175 nm (SD ±48). In contrast, Cu(ABDC-PS)(DMF) predominantly yielded nanosheets which were consistently ~1.4 nm thick, corresponding to a single layer. A few fragments of partially exfoliated material were observed ranging between 15 and 120 nm. The functionalised nanosheets were typically larger and had a broader size distribution than those of the unfunctionalised MOFs, with an average lateral size of 344 nm (±205). The shapes of the functionalised nanosheets also appear less geometric, most likely a result of the increased fragility of the structures as they approach monolayer thickness.

This trend in size distribution was also observed in DLS data (fig. S15), wherein the Cu(ABDC-PS)(DMF) MON exhibited a larger average size with a broader distribution than the Cu(ABDC)(DMF) MON. Although the DLS data indicates smaller average nanosheet sizes than those observed *via* AFM for both systems, this is consistent with previous studies which have shown that DLS underestimates particle sizes of materials with sheet morphologies.[35]

The functionalised nanosheets were isolated from suspension by centrifugation at 4500 rpm for 3 hours. The FT-IR spectrum indicated no chemical change in comparison to the functionalised MOF (fig. S23), and PXRD analysis of the nanosheets indicated that the layered framework had been maintained (fig. S14). It is interesting to note that despite monolayer formation, well defined peaks are observed which indicates repacking is taking place upon sedimentation. Minor additional peaks at 6, 8 and 50° are also observed in XRPD patterns of the PSF-MONs following exfoliation in acetonitrile. Soaking of the MONs in DMF removes these peaks which are attributed to a desolvated phase as has previously been observed for related systems (fig. S13-14).[18,19] Proton NMR spectroscopy of the digested MONs showed an increased conversion from 17 to ~ 23% (fig. S23), suggesting the more

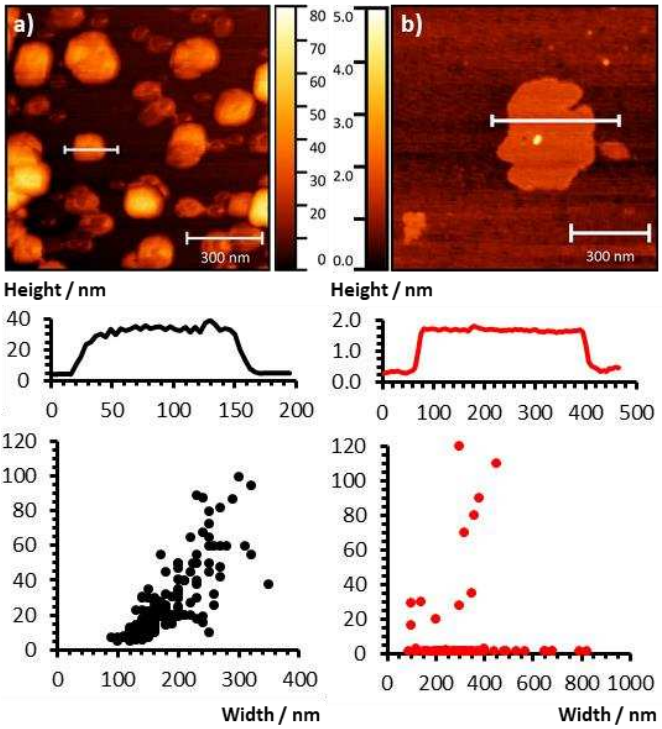

Figure 2. AFM topographical images, associated height profiles and respective size distribution scatter plots of a) Cu(ABDC)(DMF) nanosheets and b) Cu(ABDC-PS)(DMF) nanosheets. Further imaging data can be found in the ESI, figs. S19-22.

functionalised layers of the MOF had preferentially exfoliated and retained better in suspension.

Zeta potential analysis of both Cu(ABDC)(DMF) and Cu(ABDC-PS) MONs gave values of -23.0 mV and -39.6 mV respectively (also see table S2). This indicates that addition of the sulfonate groups produces nanosheets with a larger negative surface charge. In the MOF, this excess of negative charge could lead to repulsive interlayer interactions aiding exfoliation during sonication resulting in the thinner nanosheets observed by AFM. Contact angle measurements for drops of acetonitrile on a mica sheet coated with Cu(ABDC-PS) or Cu(ABDC)(DMF) were 7.0° and 12.5° respectively. This suggesting the surface energy of the PSF-MON matches more closely with acetonitrile, which could further drive the formation of observed ultrathin nanosheets and improve the stability of larger sheets in suspension.

The use of catalysts for tandem reactions in which multiple distinct active sites catalyse sequential steps in a reaction has recently received considerable attention as a means of producing greener catalysts. There has been growing interest in the use of MOFs for tandem catalysis[36–38] with recent reports of MONs being used alongside nanoparticles and enzymes to facilitate multistep reactions.[9,10,39] As Cu(ABDC-PS) is partially functionalised with sulfonic acid groups, with basic amine sites remaining, we decided to investigate their ability to catalyse a well-known acid-base tandem reaction.[34,40,41]

Cu(ABDC-PS) was tested as a catalyst for the acid hydrolysis of benzaldehyde dimethyl acetal (1) to benzaldehyde (2), followed by a Knoevenagel condensation to form benzylidene malononitrile (3). The results of the catalytic experiments after

Table 1: Reaction scheme and catalytic data for the acid hydrolysis of benzaldehyde dimethyl acetal (1) to benzaldehyde (2), followed by base-catalysed Knoevenagel condensation of benzaldehyde with malononitrile (3) to form nitrostyrene. All experiments were performed at 60 °C in d_3-acetonitrile for 24 hours. a. 0.1 mol% added before filtration (figs. S25-31).

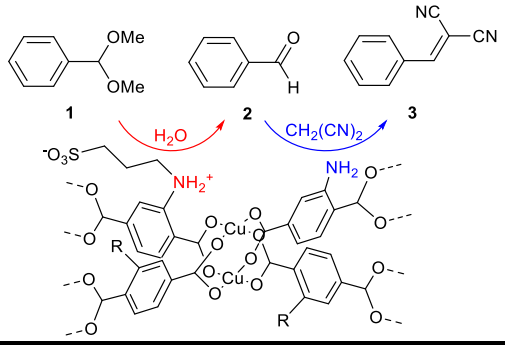

Catalyst	Type	[Cat.] / mol%	Product / %		
			1	2	3
No Catalyst	-	0	78	21	1
Cu(ABDC)	MOF	0.2	70	28	2
Cu(ABDC)	MON	0.1	56	42	2
Cu(ABDC-PS)	MOF	0.2	62	35	3
Cu(ABDC-PS)	MON	0.1	0	18	82
Cu(ABDC-PS) post-filtration	MON	0.1[a]	65	32	3
Cu(ABDC-PS), recycled	MON	1.5	0 0	14 21	86 79

24 h at 60°C and those of the corresponding PSF-MOF, and unfunctionalised MOF and MON are shown in table 1. Only Cu(ABDC-PS) was able to catalyse both acid and base reactions to any significant degree, with conversion to 82% of **3** after 24 hours with the remaining material being the intermediate **2**. In contrast, unexfoliated PSF-MOF produced only 3% conversion to **3** demonstrating the rate enhancement caused by the vastly higher surface area following exfoliation to nanosheets. The unfunctionalised MOF and MON produced less than 2% of this product demonstrating the role of the PSF group in facilitating the reaction.

A detailed analysis is beyond the scope of this paper but previous studies indicate that, as highlighted in the scheme above table 1, the ligand is zwitterionic with the secondary and primary amines acting as acid and base respectively.[34] The acid catalysed reaction had a relatively high background rate with 21 % conversion to **2** over the reaction period. Interestingly this step is enhanced by the presence of all of the references, including the unfunctionalised MOF (35 %) and MON (42%), which could indicate a role for the Lewis acidic axial sites in facilitating this reaction.[42]

The heterogeneous nature of the catalyst and its recyclability were tested. The reaction mixture including the nanosheet suspension was filtered through a 0.2 µm GHP filter before heating for 24 hours. UV-Vis spectroscopy indicated a concentration of <0.01 $mgmL^{-1}$ after filtration with no Tyndall scattering observed (fig. S27). Analysis of the reaction mixture after 24 h indicates a significantly reduced yield of 3% for **3** and

32% of **2** confirming that the catalyst is heterogeneous. In order to demonstrate recyclability, the concentration of MONs was increased to 1.5 mol% to allow the nanosheets to be washed during recovery. The initial reaction proceeded as previously giving 86 % conversion to **3**. The mixture was then centrifuged for 3 h at 4500 rpm and washed with acetonitrile. The nanosheets were redispersed in fresh reaction mixture, allowed to proceed and gave conversion to **3** of 79% (Fig. S28) showing the nanosheets can be reused.

In conclusion, we have demonstrated that covalent post-synthetic functionalisation of layered MOFs can be used to enhance their top-down exfoliation into monolayer nanosheets and to impart catalytic activity. The layered MOF, Cu(ABDC)(DMF) was reacted with 1,3-propanesultone resulting in 17% functionalisation after 1 week due to its relatively dense structure. Ultrasonic exfoliation in acetonitrile produced larger, predominantly monolayer (1.4 nm) nanosheets, in contrast to the broad thickness distribution (25 nm ±19) and smaller lateral dimensions observed for the unfunctionalised system. The higher aspect ratio of the PSF MON is attributed to electrostatic repulsion between the negatively charged sulfonate groups, weakening interlayer interactions leading to enhanced exfoliation during sonication and improved solvent-MON interactions reducing the loss of larger nanosheets from suspension during centrifugation. The partially functionalised MONs were found to catalyse the acid-base deacetylation-Knoevenagel condensation reaction in contrast to their unfunctionalised and unexfoliated counterparts. We anticipate that covalent PSF will be broadly applicable to enhancing the exfoliation of a range of layered MOFs and for introducing 'active' functional groups onto the surface of MONs to enable catalysis, sensing, separation and electronic applications.

Notes and references

1 D. J. Ashworth and J. A. Foster, *J. Mater. Chem. A*, 2018, **6**, 16292–16307.
2 M. Zhao, Y. Huang, Y. Peng, Z. Huang, Q. Ma and H. Zhang, *Chem. Soc. Rev.*, 2018, **47**, 6267–6295.
3 M. Xu, S. S. Yang and Z. Y. Gu, *Chem.- A Eur. J.*, 2018, 15131.
4 W. Zhao, J. Peng, W. Wang, S. Liu, Q. Zhao and W. Huang, *Coord. Chem. Rev.*, 2018, **377**, 44–63.
5 A. Mukhopadhyay, V. K. Maka, G. Savitha and J. N. Moorthy, *Chem*, 2018, **4**, 1059–1079.
6 L. Cao, Z. Lin, F. Peng, W. Wang, R. Huang, C. Wang, J. Yan, J. Liang, Z. Zhang, T. Zhang, L. Long, J. Sun and W. Lin, *Angew. Chemie - Int. Ed.*, 2016, **55**, 4962–4966.
7 Y. Wang, M. Zhao, J. Ping, B. Chen, X. Cao, Y. Huang, C. Tan, Q. Ma, S. Wu, Y. Yu, Q. Lu, J. Chen, W. Zhao, Y. Ying and H. Zhang, *Adv. Mater.*, 2016, **28**, 4149–4155.
8 R. Dong, Z. Zheng, D. C. Tranca, J. Zhang, N. Chandrasekhar, S. Liu, X. Zhuang, G. Seifert and X. Feng, *Chem. - A Eur. J.*, 2017, **23**, 2255–2260.
9 P. Ling, C. Qian, F. Gao and J. Lei, *Chem. Commun.*, 2018, **54**, 11176–11179.
10 Y. Huang, M. Zhao, S. Han, Z. Lai, J. Yang, C. Tan, Q. Ma, Q. Lu, J. Chen, X. Zhang, Z. Zhang, B. Li, B. Chen, Y. Zong and H. Zhang, *Adv. Mater.*, 2017, **29**, 1–5.
11 J.-X. Wu, S.-Z. Hou, X.-D. Zhang, M. Xu, H.-F. Yang, P.-S. Cao and Z.-Y. Gu, *Chem. Sci.*, 2019, **10**, 2199–2205.
12 Z. Xia, J. Fang, X. Zhang, L. Fan, A. J. Barlow, T. Lin, S. Wang, G. G. Wallace, G. Sun and X. Wang, *Appl. Catal. B Environ.*, 2019, **245**, 389–398.
13 J. Huang, Y. Li, R. K. Huang, C. T. He, L. Gong, Q. Hu, L. Wang, Y. T. Xu, X. Y. Tian, S. Y. Liu, Z. M. Ye, F. Wang, D. D. Zhou, W. X. Zhang and J. P. Zhang, *Angew. Chemie - Int. Ed.*, 2018, **57**, 4632–4636.
14 T. He, B. Ni, S. Zhang, Y. Gong, H. Wang, L. Gu, J. Zhuang, W. Hu and X. Wang, *Small*, 2018, **14**, 1–6.
15 Z. Q. Li, L. G. Qiu, W. Wang, T. Xu, Y. Wu and X. Jiang, *Inorg. Chem. Commun.*, 2008, **11**, 1375–1377.
16 P.-Z. Li, Y. Maeda and Q. Xu, *Chem. Commun.*, 2011, **47**, 8436.
17 H. Xu, J. Gao, X. Qian, J. Wang, H. He, Y. Cui, Y. Yang, Z. Wang and G. Qian, *J. Mater. Chem. A*, 2016, **4**, 10900–10905.
18 J. A. Foster, S. Henke, A. Schneemann, R. A. Fischer and A. K. Cheetham, *Chem. Commun.*, 2016, **52**, 10474–10477.
19 L. D. Smith, J. A. Foster, R. W. M. Al-Saedi, A. J. H. M. Meijer, A. Cooper, M. Trueman and D. J. Ashworth, *Chem. – A Eur. J.*, 2018, **24**, 17986–17996.
20 X. Wang, C. Chi, K. Zhang, Y. Qian, K. M. Gupta, Z. Kang, J. Jiang and D. Zhao, *Nat. Commun.*, 2017, **8**, 14460.
21 Y. Peng, Y. Li, Y. Ban, H. Jin, W. Jiao, X. Liu and W. Yang, .
22 Y. Zhou, M. Zhang, Z. Guo, L. Miao, S. T. Han, Z. Wang, X. Zhang, H. Zhang and Z. Peng, *Mater. Horizons*, 2017, **4**, 997.
23 A. Abhervé, S. Mañas-Valero, M. Clemente-León and E. Coronado, *Chem. Sci.*, 2015, **6**, 4665–4673.
24 Y. Ding, Y. P. Chen, X. Zhang, L. Chen, Z. Dong, H. L. Jiang, H. Xu and H. C. Zhou, *J. Am. Chem. Soc.*, 2017, **139**, 9136–9139.
25 W. J. Song, *Talanta*, 2017, **170**, 74–80.
26 Z. Wang and S. M. Cohen, *Chem. Soc. Rev.*, 2009, **38**, 1315.
27 K. K. Tanabe and S. M. Cohen, *Chem. Soc. Rev.*, 2011, **40**, 498–519.
28 G. Lan, Z. Li, S. S. Veroneau, Y. Y. Zhu, Z. Xu, C. Wang and W. Lin, *J. Am. Chem. Soc.*, 2018, **140**, 12369–12373.
29 W. Shi, L. Cao, H. Zhang, X. Zhou, B. An, Z. Lin, R. Dai, J. Li, C. Wang and W. Lin, *Angew. Chemie - Int. Ed.*, 2017, **56**, 9704–9709
30 Y. F. Song and L. Cronin, *Angew. Chemie - Int. Ed.*, 2008, **47**, 4635–4637.
31 S. M. Cohen, *Chem. Rev.*, 2012, **112**, 970–1000.
32 R. S. Andriamitantsoa, J. Wang, W. Dong, H. Gao and G. Wang, *RSC Adv.*, 2016, **6**, 35135–35143.
33 M. Köppen, O. Beyer, S. Wuttke, U. Lüning and N. Stock, *Dalt. Trans.*, 2017, **46**, 8658–8663.
34 H. Liu, F. G. Xi, W. Sun, N. N. Yang and E. Q. Gao, *Inorg. Chem.*, 2016, **55**, 5753–5755.
35 M. Lotya, A. Rakovich, J. F. Donegan and J. N. Coleman, *Nanotechnology*, 2013, **24**, 265703.
36 Y. B. Huang, J. Liang, X. S. Wang and R. Cao, *Chem. Soc. Rev.*, 2017, **46**, 126–157.
37 S. M. J. Rogge, A. Bavykina, J. Hajek, H. Garcia, A. I. Olivos-Suarez, A. Sepúlveda-Escribano, A. Vimont, G. Clet, P. Bazin, F. Kapteijn, M. Daturi, E. V. Ramos-Fernandez, F. X. I. Llabrés Xamena, V. Van Speybroeck and J. Gascon, *Chem. Soc. Rev.*, 2017, **46**, 3134–3184.
38 A. H. Chughtai, N. Ahmad, H. A. Younus, A. Laypkov and F. Verpoort, *Chem. Soc. Rev.*, 2015, **44**, 6804–6849.
39 L. Ye, Y. Gao, S. Cao, H. Chen, Y. Yao, J. Hou and L. Sun, *Appl. Catal. B Environ.*, 2018, **227**, 54–60.
40 H. He, F. Sun, B. Aguila, J. A. Perman, S. Ma and G. Zhu, *J. Mater. Chem. A*, 2016, **4**, 15240–15246.
41 J. Park, J. R. Li, Y. P. Chen, J. Yu, A. A. Yakovenko, Z. U. Wang, L. B. Sun, P. B. Balbuena and H. C. Zhou, *Chem. Commun.*, 2012, **48**, 9995–9997.
42 R. Natarajan, M. Yoon, Y. Ho Ko, K. Kim, R. Srirambalaji, S. Hong, Y. Kim and R. Hota, *Chem. Commun.*, 2012, **48**, 11650.

